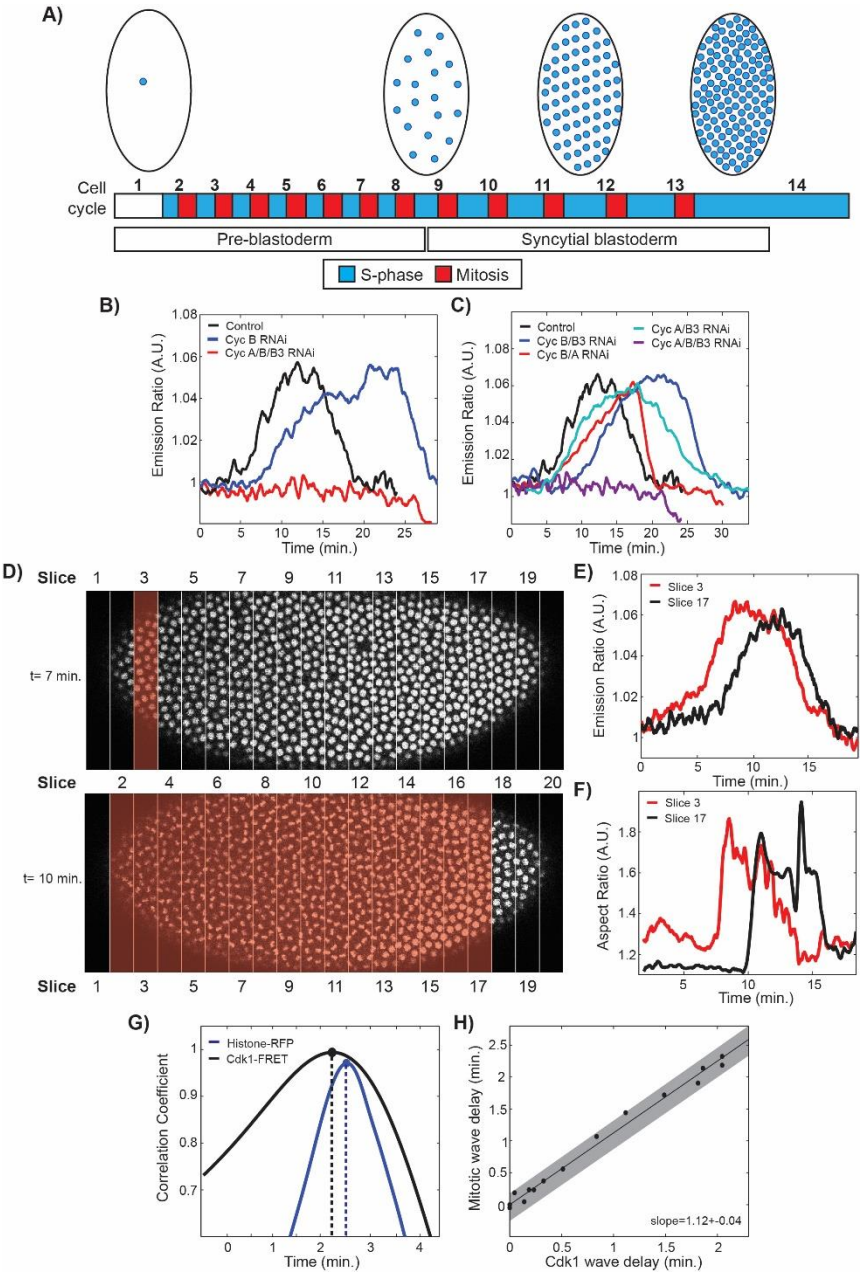

Figure S1. Validation of the Cdk1 FRET sensor and computational method to calculate wave speed. (A) Schematic of early development in *Drosophila*. (B) Cdk1 sensor is not specific to cyclin B-Cdk1 complexes. (C) Cdk1 sensor responds to the activity of all three cyclin-Cdk1 complexes as indicated by pairwise knockdown of cyclins. Triple knockdown results in an arrested cell cycle and failure of the Cdk1 sensor to detect any changes in FRET efficiency. Control indicates dye injection. (D) Images of His2Av-RFP embryos that were divided into 20 vertical slices along the AP-axis. Red shaded box represents area where nuclei are transitioning between slow and fast Cdk1 ramp-up. (E) Cdk1 FRET sensor emission ratio for slice 3 (red) and slice 17 (black). (F) Aspect ratio of nuclei estimated from His2Av-RFP images for slice 3 (red) and slice 17 (black). (G) Correlation coefficient analysis using slice 3 and 17 for His2Av-RFP (blue) and Cdk1-FRET (black) images. Shaded circle represents local maximum and dotted line corresponds to the time delay at which the correlation coefficient is at its maximum. (H) Mitotic wave delay versus Cdk1 wave delay for all slices in one embryo. Related to Figure 1.

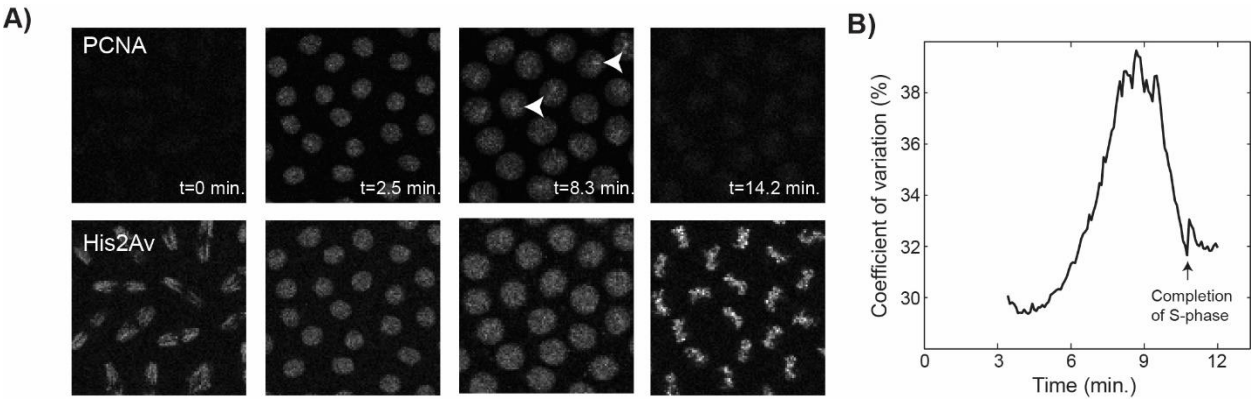

Figure S2. **PCNA-TagRFP as a marker of completion of S-phase**. (A) Top panel shows time-lapse images of PCNA-TagRFP, which localizes to foci in late S-phase (arrowheads). Lower panel shows His2Av-GFP signal as a reference to mitotic events. (B) Coefficient of variation (ratio of standard deviation to mean of intensity signal) for all nuclei in an embryo. Completion of S-phase was identified as the point when the coefficient of variation returns to a basal interphase level. Related to Figure 2.

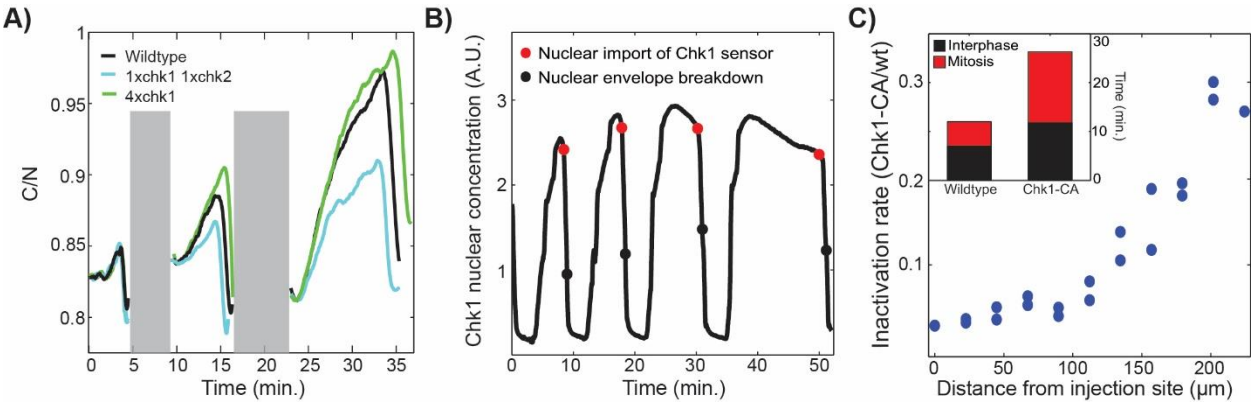

Figure S3. Validation of the Chk1 sensor. (A) Cytoplasmic to Nuclear (C/N) intensity ratio of the sensor ratio in wild type vs. *1xchk11xchk2* (blue) and *4xchk1* (green) mutants. One copy of Chk1-TagRFP-T expressed from the maternal tubulin promoter -and spaghetti squash 3' UTR- should result in Chk1 protein levels similar to wild type levels. Embryos expressing Chk1-TagRFP-T were therefore labelled as *4xchk1*. Grey shaded box represents mitosis, when the absence of nuclear envelope precludes a reliable measure of the C/N ratio. (B) Chk1 nuclear concentration-using a Chk1-TagRFP-T construct- as a function of time (cycles 10-13). The red and black dots indicate the time of inactivation of the sensor and of nuclear envelope breakdown. (C) The rate of inactivation of the sensor is inversely proportional to the distance from the site of injection of Chk1-CA mRNA. Inset: estimated cell cycle duration for wild type and Chk1-CA. Related to Figure 4.

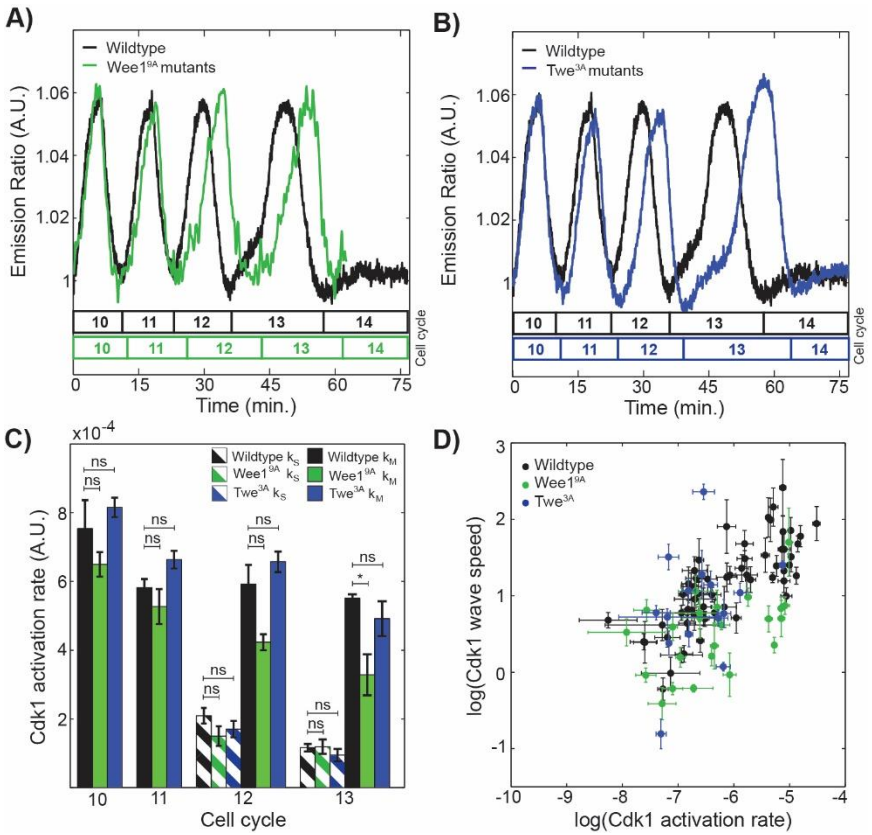

Figure S4. **Positive feedback from the Cdk1 mitotic circuit regulates abruptness of Cdk1 activation.** (A) Emission ratio of Cdk1 sensor for wildtype embryos (black line) and *wee1*^{9A} embryos (green line). (B) Emission ratio of Cdk1 sensor for wildtype embryos (black line) and *twe*^{3A} embryos (blue line). (C) Average Cdk1 activation rate per cell cycle for wildtype (black), *wee1-9A* (green), and *twine-3A* (blue) embryos. Error bars, s.e.m., ***, $p<0.0001$; *, $p<0.05$; ns, not significant. (D) Log-log plot of Cdk1 speed versus S-phase Cdk1 activation rate for wildtype (black), *wee1-9A* (green), and *twine-3A* (blue) embryos. Error bars, 95% CI. Related to Figure 5.

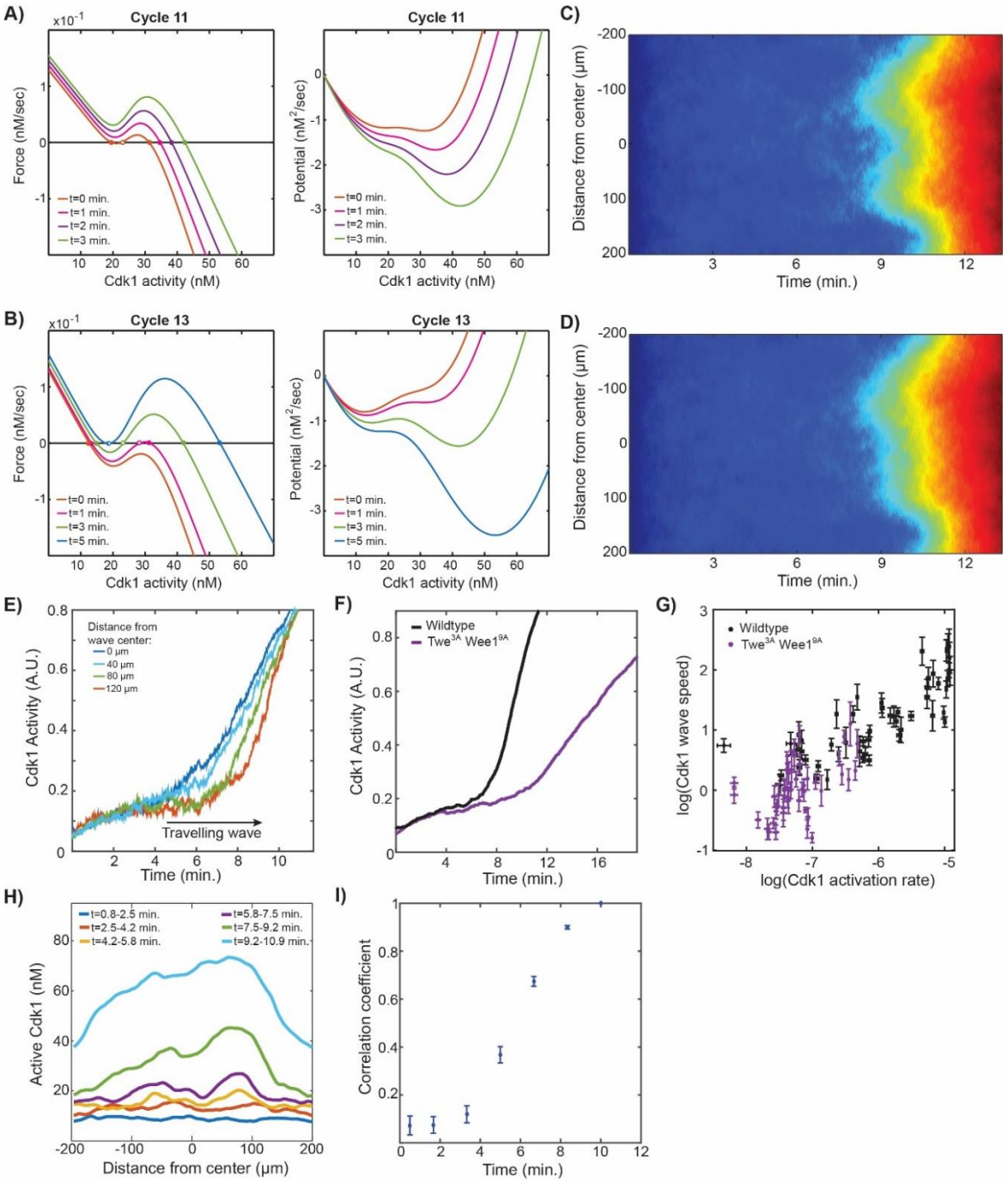

Figure S5. Mathematical modelling of Cdk1 waves. (A-B) Plot of the force (left) and the potential (right) as a function of active Cdk1 for different times during cycle 11 (A) and cycle 13 (B). (C-D) We show the field *a(x,t)* as computed from simulations of the effective equation (See equation 3 in Supplemental Information) (C) or from simulations of the complete equations (See equation 1 in Supplemental Information) (D). We used the same Gaussian noise for both simulations, which show very similar fields. (E) The time-profile of the Cdk1 activity for four different positions along the AP-axis versus time. (F) Cdk1 activity profile for wild type (black) and *twe*^{3A} *wee1*^{9A} (purple) phenotypes. (G) Log-log plot of Cdk1 speed versus S-phase Cdk1 activation rate for simulations of the wild type (black) and simulations of the *twe*^{3A} *wee1*^{9A} mutants (purple). Error bars, 95% CI. (H) Spatial profiles of Cdk1 activity averaged over different time intervals. (I) Correlation coefficient between the average field between 9.2-10.9 minutes and the fields at previous times. Related to Figure 6.

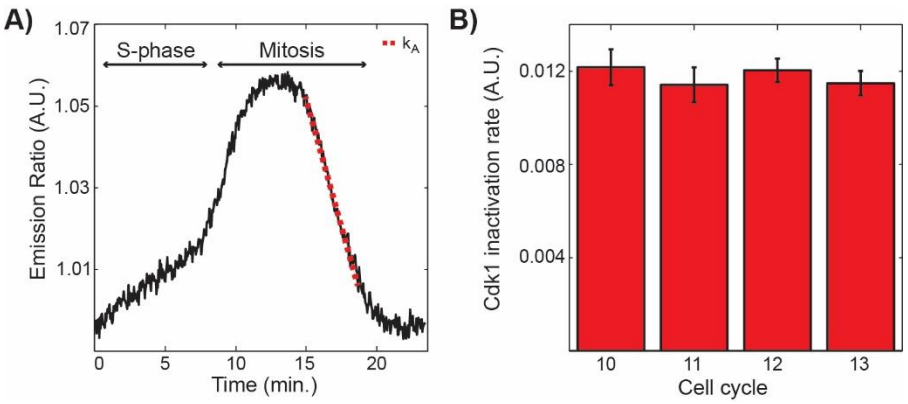

Figure S6. The rate of inactivation of Cdk1 during anaphase does not change during development. (A) Emission ratio of Cdk1 sensor for cycle 13. The dotted line indicates the linear fit to extract the rate of Cdk1 inactivation. (B) Rate of Cdk1 inactivation as a function of cell cycle number. Error bars, s.e.m. Related to Figure 7.

Table S1. Values of the parameters used for numerical simulations of the model. Related to Figure 6.

Parameters	**Value**
D_{Chk1}, D_{Cdk1}	4.3 $\mu m^2/s$
K_{Chk1}	30 nM
α	8 nM/min
c_0	0.12 min^{-1}
c_1	0.6 min^{-1}
K_{Cdc25}, K_{Wee1}	40 nM
f_{max}	1
r_0	60/7 min^{-1}
w_0	0.2 min^{-1}
w_1	1 min^{-1}
$\Gamma_a=\Gamma_f$	5.3 $nM^{1/2}$
σ	10
ν, μ	5

Supplemental Movie Legends

Movie S1. Mitotic waves in the early *Drosophila* embryo. Time-lapse video of an embryo expressing His2AvRFP during cell cycles 10-13. Mitotic waves are initiated at the poles and become less synchronous as development progresses. Images were acquired with 1/2.79 s. frame rate and are shown at 50 frames/s. Related to Figure 1.

Movie S2. Embryo ligation during cycles 8-9 results in asynchronous mitotic waves in anterior versus posterior compartments. Time-lapse video of a ligated embryo expressing His2AvRFP. Embryo was ligated at the center of the anterior-posterior axis during cycles 8-9 for 10 min., which introduced a ligation barrier. Blade was then removed and embryo was transferred to a slide for imaging. Images were acquired with 1/2.79 s. frame rate and are shown at 50 frames/s. Related to Figure 1.

Movie S3. *chk1/chk2* embryos fail to slow down cell cycles. Time-lapse video of a Chk1/Chk2-null embryo expressing His2AvRFP during cell cycles 11-13. Images were acquired with 1/2.79 s. frame rate and are shown at 50 frames/s. Related to Figure 4.

Movie S4. twe^{3A} $wee1^{9A}$ embryos generate mitotic waves. Time-lapse video of a mitotic switch mutant embryo expressing His2AvRFP during cell cycle 13. Images were acquired with 1/2.79 s. frame rate and are shown at 50 frames/s. Related to Figure 5.

Movie S5. Introducing an impermeable barrier during S-phase uncouples mitotic wave in anterior versus posterior compartments. Time-lapse video of an embryo expressing His2AvRFP that was ligated during S-phase. Images were acquired with 1/2.79 s. frame rate and are shown at 50 frames/s. Related to Figure 7.

Movie S6. Introducing an impermeable barrier during M-phase does not impede mitotic wave. Time-lapse video of an embryo expressing His2AvRFP that was ligated during early M-phase. Images were acquired with 1/2.79 s. frame rate and are shown at 50 frames/s. Related to Figure 7.

Supplemental Experimental Procedures

Stocks

Experiment	Genotype
Cdk1 waves	w; Cdk1-FRET; His2Av-mRFP
Cdk1 waves	His2Av-mRFP; grp^{209} lok^{30}/$grp^{z5170}lok^{30}$; Cdk1-FRET
Cdk1 waves	His2Av-mRFP; $wee1^{ES1}$/Df(2L)Dwee1-W05; Cdk1-FRET
Cdk1 waves	w; Cdk1-FRET twe^{HB5} twe^{3A}; His2Av-mRFP
Cdk1 waves	w; $wee1^{ES1}$ twe^{HB5} twe^{3A}/Df(2L)Dwee1-W05 twe^{HB5} twe^{3A}; Cdk1-FRET His2Av-mRFP/twepr-wee19A
Cdk1 waves	His2Av-mRFP; $wee1^{ES1}$/Def(wee1); Cdk1-FRET/ twepr-wee19A
Cdk1 Diffusion	UAS-Cdk1-Venus/nos-Gal4 (the UAS-Cdk1-Venus was a kind gift of Shelagh Campbell)
S-phase duration	w; His2Av-GFP; PCNA-TagRFP-T
Chk1 activity and waves	w; His2Av-mRFP/+; $Cdc25C^{183-251}$-EGFP/+
Chk1 activity and waves	w; grp^{209} lok^{30}/grp^{z5170} lok^{30}; $Cdc25C^{183-251}$-EGFP/His2Av-mRFP
Chk1 activity and waves	w; grp^{209} lok^{30}/+; $Cdc25C^{183-251}$-EGFP/His2Av-mRFP
Chk1 activity and waves	w; +/grp^{z5170} lok^{30}; $Cdc25C^{183-251}$-EGFP/His2Av-mRFP
Chk1 activity and waves	w; $Cdc25C^{183-251}$-EGFP/Chk1-TagRFP-T
Cdk1 activity as a function of DNA content	w; Cdk1-FRET; His2Av-mRFP females crossed to C(2)EN males (stocks BDSC 2974, BDSC 1020 and BDSC 1112)
Cdk1 activity as a function of DNA content	w; Cdk1-FRET; His2Av-mRFP females crossed to C(3)EN males (stock BDSC 1117).

Mathematical modelling of Cdk1 spreading

To further understand the regulation of the mitotic waves, we developed a mathematical model for the activity of Cdk1 and its modulation by Chk1. We first determined the important geometrical features of Cdk1 waves. The syncytial blastoderm is a multinucleated cell with the great majority of nuclei arranged on the cell surface, implying that waves essentially travel across a two-dimensional surface. Live imaging experiments show waves propagating along the anterior-posterior (AP) axis of the embryo. To determine whether the behavior of the wave can be simplified by just analyzing the propagation across the AP axis, we determined the effect of curvature on the speed of Cdk1 waves. As discussed previously (Tyson and Keener, 1988), curvature modifies the velocity v_{1D} of a rectilinear wave by terms proportional to D/R, where D is the diffusion coefficient of the chemical transported by the wave and R is the radius of curvature of the wavefront. Curvature effects are negligible when the radius of curvature R is much larger than the diffusive length $D/v_{1D,}$ the length over which the chemical diffuses in the time for the wave to propagate. Since the diffusion coefficient of Cdk1 is about 4-5 $\mu m^2/s$ and v_{1D} is in the range 2-6 μm/s, it follows that the diffusive length is on the order of microns. We conclude that the behavior of Cdk1 waves propagating in the AP direction along the surface of the embryo is well described by a one-dimensional wave along the AP axis.

Definition of the model

Chk1 regulates Cdk1 by modulating the activities of Cdc25 (inhibition) and Wee1 (activation). Following the approach described in (Chang and Ferrell, 2013), we use a single effective equation to describe the dynamics of active Cdk1 and its regulation by Wee1 and Cdc25 (see below). Conversely, Cdk1 regulates Chk1 activity by triggering its rapid inactivation at completion of S-phase and it has a clear role in regulating the timing of S-phase in early *Drosophila* embryos (Farrell et al., 2012). Therefore, we decided to include an additional equation to explicitly account for the activity of Chk1 and to capture the dependence on the cycles. The inactivation of Chk1 by Cdk1 activity is modeled by an empirical switch-like function. The inclusion of diffusion and noise finally yields the following partial-differential stochastic equations:

$$
\begin{aligned}
\frac{\partial f}{\partial t} &= D_{Chk1}\frac{\partial^2 f}{\partial x^2} - \frac{a^\sigma}{K_{Chk1}^\sigma + a^\sigma} r_0 f + \xi_f(x,t) \\
\frac{\partial a}{\partial t} &= D_{Cdk1}\frac{\partial^2 a}{\partial x^2} + \alpha + r_+(a,f)(c(x,t)-a) - r_-(a,f)a + \xi_c(x,t) + \xi_r(x,t) \qquad (1) \\
\frac{\partial c}{\partial t} &= D_{Cdk1}\frac{\partial^2 c}{\partial x^2} + \alpha + \xi_c(x,t)
\end{aligned}
$$

Here, the field *a(x,t)* denotes the amount of active Cdk1 and the field *f(x,t)* describes the modulation of Cdk1 activity due to Chk1. The space variable *x* has a single component and the model is one-dimensional because curvature effects are small.

As mentioned above, the inhibition of Cdk1 activity by Cdc25 and its activation by Wee1 are effectively taken into account via the two Hills functions:

$$
\begin{aligned}
r_+(a,f) &= \left(c_0 + c_1 \frac{a^\nu}{K_{Cdc25}^\nu + a^\nu}\right)(f_{max} - f) \\
r_-(a,f) &= \left(w_0 + w_1 \frac{K_{Wee1}^\mu}{K_{Wee1}^\mu + a^\mu}\right) f
\end{aligned}
$$

The two expressions above are as in (Chang and Ferrell, 2013), except for the explicit dependence on *f*, which is crucial for capturing the dependence on cell cycles.

The field *c(x,t)* in Eq. (1) denotes the total amount of Cdk1 complex -phosphorylated on Y15 or active. While the field depends a priori on space, the noise contribution is effectively smoothed out by diffusion: at the time of the triggering of Cdk1 waves, the field *c(x,t)* has correlations that extend over relatively large fractions of the size of the embryo. Therefore, it is safe to neglect the spatial dependency of the field and we found it convenient to drop the last line in Eq. (1) and to take for simplicity *c(x,t)=c(t)* in the second equation for *a(x,t)*. We explicitly verified that including the additional equation for *c(x,t)* does not modify the results described in the main text and below. As for the time-dependence of the average amount, we take *c(t)=αt*, where the production rate *α* is discussed below.

The mutually independent Gaussian fields ξ_f, ξ_c and ξ_r appearing in Eq. (1) are short-correlated in space and time:

$$
\begin{aligned}
<\xi_f(x,t)\xi_f(x',t')> &= 2\Gamma_f^2 \left(\frac{a^\sigma}{K_{Chk1}^\sigma + a^\sigma} r_0 f\right)\delta(x-x')\delta(t-t') \\
<\xi_c(x,t)\xi_c(x',t')> &= 2\Gamma_c^2 \alpha \delta(x-x')\delta(t-t') \qquad (2) \\
<\xi_r(x,t)\xi_r(x',t')> &= 2\Gamma_r^2 \left(r_+(a,f)(c(x,t)-a) + r_-(a,f)a\right)\delta(x-x')\delta(t-t')
\end{aligned}
$$

and they represent the effect of the noise in the chemical reactions (Gillespie, 2007). The factors Γ_f, Γ_c and Γ_r are proportionality constants. When the third equation for *c(x,t)* is neglected, the two noise terms in the equation for active Cdk1 *a(x,t)* are collapsed into a single Gaussian noise having the variance proportional to the sum of the variances:

$$
<\xi_a(x,t)\xi_a(x',t')> = \quad 2\Gamma_a^2 \left(\alpha + r_+(a,f)\left(c(t)-a\right) + r_-(a,f)a\right)\delta(x-x')\delta(t-t')
$$

The production rate *α* which appears in Eq. (1) and in the total amount of Cdk1 complex *c(t)*, is supposed constant. This term is empirically based on the observation that in embryos mutant for Chk1/Chk2 or Wee1, the activity of Cdk1 in interphase increases in a linear manner throughout development. While we expect that the synthesis of cyclins gives a contribution to this term, other biological processes probably contribute. For example, in spite of the incomplete cyclin degradation at the end of the early cycles, the activity of Cdk1 drops essentially to zero (see Figure 1). This result suggests that other processes contribute to the inactivation of Cdk1 at the end of mitosis (for example loss of activating phosphorylation on Thr161) and the consequent reactivation during interphase (phosphorylation of Thr161).

The diverse cell cycle profiles shown in the figures that we reported were obtained using the following initial values for the Chk1 modulation field *f(x,0)*: 0.25, 0.35, 0.45 and 0.55 for cycles 10, 11, 12 and 13 respectively. The diffusion constants were directly measured by the FRAP experiments discussed in the main text.

Results of simulations for the wild-type

The qualitative dynamics of the model described above goes as follows. Both *a(x,t)* and *c(t)* are initially vanishing while *f(x,t)* is set at a level that depends on the cell cycle, as described above. Then, the linear increase of *c(t)* and the production term *α* drive up the levels of *a*. The overall level of *f* remains essentially constant until the level of the field *a* approaches the threshold K_{chk1}, when the Hill function decay term in the equation for *f* starts to become important. The initial rate of growth of the field *a* is sensitive to the level *f* of Chk1 via the dependencies appearing in $r_+(a)$ and

r(a). In particular, increasingly high values of *f* lead to slower rates of growth of *a*, in agreement with experimental observations of Cdk1 time-profiles reported in the main text.

As the levels of the field *a(x,t)* become comparable to K_{chk1}, an abrupt switch occurs: Chk1 rapidly drops to zero (see Figure 6B) and wave-like transport of Cdk1 is triggered, which rapidly spreads and builds up correlations throughout the embryo (see Figures S5H-S5I). To gain an intuition on this process, it is useful to remark that variations of *f* are rapid and driven by the levels of *a*, i.e. *f* is essentially slaved to *a*. We can therefore define an effective dynamics for the field *a(x,t)* alone as:

$$\frac{\partial a}{\partial t} = D_{Cdk1}\nabla^2 a - \frac{\partial V(a)}{\partial a} + \xi_{eff}(x,t) \qquad (3)$$

where the effective potential *V(a)* and the corresponding force $-\partial_a V$ are given by

$$-\frac{\partial V}{\partial a} = \alpha + \left(c_0 + c_1 \frac{a^\nu}{K_{Cdc25}^\nu + a^\nu}\right)\left(f_{max} - f_0 \frac{K_f^\tau}{K_f^\tau + a^\tau}\right)(c(t) - a) - \left(w_0 + w_1 \frac{K_{Wee1}^\mu}{K_{Wee1}^\mu + a^\mu}\right) f_0 \frac{K_f^\tau}{K_f^\tau + a^\tau} a$$

and they are shown in Figures S5A-S5B. The parameter f_0 reflects the initial value of Chk1 activity, which depends on the cell cycle as detailed above. The two parameters K_f and τ of the Hill functions in the effective potential were derived empirically comparing the dynamics of the effective equation (3) and the dynamics of the full equations (1) for each cell cycle.

Two remarks are worth: (i) the reaction terms in the original equations (1) are not of the gradient type, as can be checked by calculating their curl, which does not vanish; (ii) The expression of *f* as a function of *a* that is used to construct the potential *V(a)* depends on the cell cycle and *V(a)* is therefore different for the various cycles. A typical comparison of the fields *a(x,t)* obtained by the numerical simulations of the original two-species equation (1) and the effective equation (3) is shown in Figures S5C-S5D. While some slight differences are visible, the two fields are very similar, which provides a concrete sense of the validity of the effective potential approximation.

For initial values of *f* larger than about 0.35, the effective potential *V(a)* has multiple extrema (Figures S5A-S5B), i.e. the force field has multiple zeros. The size of the bistable region increases with the initial level of *f*. As the level of *a(x,t)* increases, a noise-induced switch eventually occurs when the amplitude of the noise becomes comparable to the distance between the low-a minimum and the maximum of the potential shown in Figures S5A-S5B. The blocking effect of Chk1 on the rate of growth of Cdk1 is then abolished, and after a short crossover period (needed to reach levels comparable to K_{Cdc25}) growth reaches its full speed. Note that the full-speed growth rate does not depend on *f* and is therefore common to all cycles, which agrees with the experimental observations that were reported in the main text. The spatial regions where *a(x,t)* has jumped the potential barrier will diffusively spread their higher values in the neighboring regions, which will catalyze their own jumping over the barrier, and so on. That constitutes the classical physical mechanism for triggering chemical waves (Chang and Ferrell, 2013; Saarloos, 1998; Tyson and Keener, 1988), which leads to the rapid wave-like spreading of Cdk1 that is observed both in numerical simulations and experiments. Finally, the fact that bistability increases with the level of *f* is in agreement with the experimental observations that early cycles are much more disordered, and that the wave-like nature of the Cdk1 spreading becomes more pronounced as cycles progress, becoming quite distinct for the very last cycles.

Once the phase of full-speed growth starts, the various nuclei interact only by diffusion, which couples them relatively locally. It follows that spatially separated embryonic regions proceed largely independently of each other. Their profiles of growth will be similar, yet shifted in time due to delay generated by the chemical Cdk1 wave. Because of the similarity of the *a(x,t)* profiles, we do not need to specify the detailed mechanism of how mitosis is controlled by the time course of *a*. For instance, mitosis could be controlled by a threshold on instantaneous levels of *a*, or by a threshold on the time integral of *a(x,t)* with an appropriate memory kernel, or by some other more complicated possibility. Irrespective of the mechanism of control, mitotic events will reflect the delays that were set by the Cdk1 chemical wave triggered at the end of the S-phase. Note that mitotic divisions will take place in a spatially coordinated manner but without any spreading of chemicals. In other words, the embryonic mitotic waves are not trigger waves but phase waves, i.e. they are kinematic and just reflect pre-defined delays among different spatial points. The nature of phase waves implies they can a priori travel at arbitrary speeds due to the absence of any causality constraint. However, delays in our case are not arbitrary as they are set by the S-phase Cdk1 trigger wave. We conclude that the velocity of the mitotic phase waves and the velocity of the S-phase trigger waves coincide, which explains the experimental observations. Still, trigger and phase waves are fundamentally different, as confirmed by the timed-ligation experiments described in the main text.

Simulations for the mitotic switch mutant

In order to describe the dynamics of the mitotic switch mutant (*twe*^{3A} *wee1*^{9A} mutant, see Figure 5), we simulated the same partial differential stochastic equations (1), but we set to zero the two parameters $c_1=w_1=0$, i.e. the Hill functions

that models the effects of Wee1 and Cdc25 are removed. We also set the parameter $w_0=1.2$ min^{-1} and found that the fit for the dependence of the speed of Cdk1 waves was slightly improved by using $r\_(a)=w_0(f+0.06)$, i.e. assuming a basal level of Wee1 activity which is independent of Chk1. This remark should be taken as an empirical observation, and we have not tried to elucidate its molecular basis. The results of the numerical simulations demonstrate that the model can reproduce the experimental observation that the rate of Cdk1 activation in mitosis, but not in S-phase, is significantly affected by mutation of the mitotic switch (Figure S5F). Moreover, the model generates waves but they are slightly slower compared to wild type (Figure S5G), which is again consistent with experimental data (Figure 5C).

In conclusion, the ensemble of the results described above for wild-type and mutants argues that our model (1) for the activity of Cdk1 explains the scaling of the speed of Cdk1 waves and capture all the main properties of the spatiotemporal dynamics of Cdk1 observed experimentally. The model also clarifies the fundamentally different nature of the waves observed at the end of the S-phase and the mitotic waves, which is illustrated by the timed-ligation experiments reported in the main text.

Analysis of the wave-like nature of the Cdk1 spreading

Experimental data of Cdk1 activity (see Figure 1 in the main text) as well as simulations of the model (Figure S5E) show that the spreading of Cdk1 activity is not exactly a wave, i.e. the wave front slightly distorts as it translates and the velocity is not quite constant. Still, the spreading is wave-like, i.e. close enough to the exact case to make ideas and techniques from waves appropriate and useful, which is what we have done throughout the paper. The scope of this section is to discuss this point in some more detail, namely present the physical reasons why there is no exact wave and why deviations are relatively small.

1) The total amount of Cdk1 complex -phosphorylated on Y15 or active - changes with time, namely its average level $c(t)$ increases linearly in time. The total amount enters the reaction terms in the equations (1) of the model and modifies the effective potential in (3), which governs the Cdk1 activity. It follows that the potential in the reaction-diffusion equation (3) is an explicit function of time. Standard formulations of the problem of wave propagation in reactive media feature an autonomous system, i.e. a time-independent potential (Saarloos, 1998; Tyson and Keener, 1988). The time-dependence of the potential makes that the profile and the velocity of the front are a priori affected and the wave distorts as it spreads because the potential modifies.

In practice, these effects turn out to be moderate as the time scale of the Cdk1 spreading across the entire embryo, which is on the order of a minute, is relatively rapid so that the typical variations of the potential over that time are not dramatic.

2) The total amount of Cdk1 complex is a function of space and is not constant over the embryo. By the same reasoning as in the point 1) above, it follows that the potential in the reaction-diffusion equation (1) depends on space. This is again expected to distort the profile and velocity of the front because the potential changes as the wave spreads across the embryo.

The effect is visible (see Figure S5E) but, similarly to the effect above of the time-dependence, it is not strong. The reason is that the space-dependence of the potential at typical times when the waves are triggered is relatively slow. Indeed, the upshot of the calculation detailed in the next Section, is that at the time when the Cdk1 wave spreads, the correlation length of the field $c(x,t)$ defined in equation (1) is smaller than the embryo size but much longer than a few microns. The scale of variation of the potential should indeed be compared to the diffusive length D/v, i.e. the length over which the chemical diffuses in the time for the wave to propagate. As already mentioned previously while estimating the effects of curvature, the diffusive length for our system is a few microns. We conclude that the local spreading of the fronts is only weakly distorted and the variation of the potential gives a large-scale modulation of the properties of the wave fronts. This conclusion is consistent with our experimental observations and the results of numerical simulations.

3) The dynamics of *Drosophila* embryos and our model is affected by noise. In addition to producing fluctuations in the space-time profiles of the various fields, namely Cdk1, noise crucially affects the timing and the mechanism for triggering the waves.

The embryonic system differs from typical configurations usually considered for wave spreading[5]. Namely, the initial field usually features a region of space prepared around the stable global minimum of the potential, and its subsequent invasion of the rest of space set at the metastable minimum of the potential is tracked. Similar initial configurations are used for simulations and experiments previously reported (Chang and Ferrell, 2013). For the previous configuration, noise affects the velocity of the wave via its contribution to the dynamics of the general reaction-diffusion equation (3), especially because the amplitude of noise is comparable to the kinetic barrier to be overcome. The velocity will then generally differ from the value for the deterministic dynamics that can be obtained via the mechanical mapping described prior (Saarloos, 1998).

The second effect of noise, which is peculiar to the actual embryonic system, relates to the fact that bistable switching is spontaneous and driven by noise. This fact has two main effects. First, the timing of the trigger fluctuates in different realizations, as confirmed by the correlations shown in Figure S5I that build up over several minutes. Fluctuations are particularly important as the potential changes in time and the kinetic barrier that must be overcome reduces as time progresses. Late switchers are therefore expected to have a higher velocity. Conversely, increasing the level of noise should anticipate the switching and thus reduce the velocity of the wave. Second, when the system switches, it does not jump directly from the metastable minimum of the potential to the globally stable minimum. The landing point and the fact that the force will generally be non-zero will again affect the rapidity of the consequent wave-like spreading.

A detailed theoretical treatment of the various physical effects that we have described above is beyond the scope of the present work and will be the object of a separate draft.

Space-time distribution of the Cdk1 complex

The amount *c(x,t)* of Cdk1 complex- phosphorylated on Y15 or active - is controlled by constant production and is not affected by the nonlinear processes of phosphorylation and dephosphorylation by Wee1 and Cdc25. Its space-time distribution can then be determined analytically as follows. The equation for the amount of complex $c(\boldsymbol{x},t)$ is:

$$\partial_t c = D\nabla^2 c(\mathbf{x},t) + \alpha + K\sqrt{\alpha}\eta(\mathbf{x},t)$$

where α is the production rate, *D* is the diffusivity, $K = \sqrt{2}\Gamma_c$ is a constant- see Eq.(2)- controlling the amplitude of the noise and η is Gaussian Langevin random noise δ-correlated in space and time $\langle \eta(\boldsymbol{x},t)\eta(\mathbf{0},0)\rangle = \delta(\boldsymbol{x})\delta(t)$ (regularized and discretized as discussed below).

Due to the linearity of the previous equation, the field *c* will be Gaussian with mean given by <*c*>= αt, i.e. the mean is constant in space and grows linearly with time.

The equal-time correlation function $C(\boldsymbol{x},t) = \langle c(\boldsymbol{x},t)c(\mathbf{0},t)\rangle - \langle c(\boldsymbol{x},t)\rangle\langle c(\mathbf{0},t)\rangle$ obeys:

$$\partial_t C = 2D\nabla^2 C(\mathbf{x},t) + 2K\sqrt{\alpha} < \eta(\mathbf{x}',t)c(\mathbf{x}'+\mathbf{x},t) >$$

where we have used spatial homogeneity to simplify the equation. Using Gaussian integration by parts (see page 43 in (Frisch and Kolmogorov, 1995)) and the δ-correlation in space and time of the Langevin noise, the equation reduces to:

$$\partial_t C = 2D\nabla^2 C(\mathbf{x},t) + K^2\alpha\delta(\mathbf{x})$$

that is, a heat equation with a source term constant in time and short-correlated in space. The solution is:

$$C(\mathbf{x},t) = K^2\alpha\int_0^t \frac{e^{-\frac{\mathbf{x}^2}{8D(t-s)}}}{(8\pi D(t-s)^{d/2}}ds$$

where *d* is the space dimensionality.

In one dimension, the value at the origin, i.e. the variance, is easily computed: $(\mathbf{0},t) = K^2\alpha\sqrt{\frac{t}{2\pi D}}$. The interesting point is that the mean is growing as *t* so as time progresses the level of fluctuations becomes smaller and smaller and the coefficient of variation decreases as $t^{-3/4}$. In two dimensions, the variance grows even more slowly $C(\mathbf{0},t) = \frac{K^2\alpha}{8\pi D}\log(t/\Delta t)$, where $\Delta t \simeq \Delta x^2/D$ is the shortest time scale in the problem and Δx is the space discretization distance, e.g. of the order of the distance among two nuclei in our case.

The asymptotic behavior at large distances $\boldsymbol{x}^2/Dt \gg 1$, is obtained as follows. The change of variable $u = \boldsymbol{x}^2/8D(t-s)$ reduces the integral to:

$$C(\mathbf{x},t) = K^2\alpha\frac{\mathbf{x}^{2-d}}{8D\pi^{d/2}}\int_{\frac{\mathbf{x}^2}{8Dt}}^{\infty} u^{\frac{d}{2}-2}e^{-u}du$$

and integration by parts gives the asymptotic behavior:

$$C(\mathbf{x},t) \simeq \frac{t^{2-d/2}}{\mathbf{x}^2\pi^{d/2}}e^{-\frac{\mathbf{x}^2}{8Dt}}$$

that is the field becomes correlated over distances growing as $\sqrt{4Dt}$ and decays rapidly beyond that scale. In our case, taking $D \simeq 5\mu m^2/s$ and timescales of the duration of interphase (4-12 minutes), the correlation length scale becomes $\sqrt{4Dt} \simeq 70 - 120\mu m$, i.e. diffusion is not fast enough to spread the signal over the entire embryo yet it reduces the

number of effectively independent regions to just a few.

The ensemble of these results accounts for two experimental observations. First, the property that nuclei are effectively coupled over relatively large distances rationalizes the experimental observation that waves typically tends to start at only 1-3 foci. Indeed, if every nucleus was trying to transition independently, many more foci might be observed given the large number of nuclei. Second, the relatively long correlations (as compared to the diffusive length of a few microns) of the Cdk1 field are important for the wave-like nature of the Cdk1, as it was discussed above.

Supplemental References

Chang, J.B., and Ferrell, J.E., Jr. (2013). Mitotic trigger waves and the spatial coordination of the Xenopus cell cycle. Nature *500*, 603-607.

Farrell, J.A., Shermoen, A.W., Yuan, K., and O'Farrell, P.H. (2012). Embryonic onset of late replication requires Cdc25 down-regulation. Genes & development *26*, 714-725.

Frisch, U., and Kolmogorov, A.N. (1995). Turbulence: The Legacy of A. N. Kolmogorov (Cambridge University Press).

Gillespie, D.T. (2007). Stochastic simulation of chemical kinetics. Annual review of physical chemistry *58*, 35-55.

van Saarloos, W. (1998). Three basic issues concerning interface dynamics in nonequilibrium pattern formation. Physics Reports *301*, 9-43.

Tyson, J.J., and Keener, J.P. (1988). Singular Perturbation Theory of Spiral Waves in Excitable Media. Physica D *32*.